Automated and Adaptable Quantification of Cellular Alignment from Microscopic Images for Tissue Engineering Applications

Feng Xu, Ph.D.,[1,*] Turker Beyazoglu, B.S.,[1,*] Evan Hefner, B.S.,[1]
Umut Atakan Gurkan, Ph.D.,[1] and Utkan Demirci, Ph.D.[1,2]

Cellular alignment plays a critical role in functional, physical, and biological characteristics of many tissue types, such as muscle, tendon, nerve, and cornea. Current efforts toward regeneration of these tissues include replicating the cellular microenvironment by developing biomaterials that facilitate cellular alignment. To assess the functional effectiveness of the engineered microenvironments, one essential criterion is quantification of cellular alignment. Therefore, there is a need for rapid, accurate, and adaptable methodologies to quantify cellular alignment for tissue engineering applications. To address this need, we developed an automated method, binarization-based extraction of alignment score (BEAS), to determine cell orientation distribution in a wide variety of microscopic images. This method combines a sequenced application of median and band-pass filters, locally adaptive thresholding approaches and image processing techniques. Cellular alignment score is obtained by applying a robust scoring algorithm to the orientation distribution. We validated the BEAS method by comparing the results with the existing approaches reported in literature (i.e., manual, radial fast Fourier transform-radial sum, and gradient based approaches). Validation results indicated that the BEAS method resulted in statistically comparable alignment scores with the manual method (coefficient of determination $R^2 = 0.92$). Therefore, the BEAS method introduced in this study could enable accurate, convenient, and adaptable evaluation of engineered tissue constructs and biomaterials in terms of cellular alignment and organization.

Introduction

Tissues and organs consist of various cell types and extracellular matrix (ECM) components well organized in three-dimensional environment that is vital to tissue function.[1] Cellular alignment is known to play an important role in neuron regeneration,[2,3] and in providing the mechanical and physical properties of tissues, such as skeletal and cardiac muscle,[4,5] arteries,[6] and tendon.[7,8] Aligned organization of cells results in deposition of a highly anisotropic ECM, which is specific to tissue type and critical in determining tissue function. For example, native smooth muscle tissue displays aligned smooth muscle cell (SMC) organization,[9] which is essential for achieving the functional mechanical strength in muscle contraction. Therefore, mimicking the native cell alignment is necessary in engineered muscle tissue (smooth, skeletal, and cardiac) to achieve effective contraction.[10] On the other hand, vascular cells are arranged in distinct patterns in the multiple layers of the arterial wall with circumferentially aligned vascular SMCs in the media and longitudinally aligned endothelial cells in the intima.[11] In the context of wound repair, axially aligned fibroblasts within the healing tissues (guided tissue regeneration) are desirable.[12] Therefore, anisotropic extracellular and cellular organization is essential in engineered connective and vascular tissue (tendons, ligaments, and blood vessels) to bestow the functional tissue strength that can withstand the physiological loads and stress.[13,14] In terms of corneal tissue, the alignment and the anisotropic organization of the ECM components and the corneal fibroblasts plays a critical role in maintaining the optical properties and the transparency.[15] Briefly, cellular alignment is critical in tissue engineering to achieve physical strength, to generate physiological level biophysical forces by cells, and to allow highly organized cellular organization (e.g., for optical transparency).

Various approaches have been developed to align cells, including topographical pattern (e.g., microgrooves),[16,17] mechanical stimulation (e.g., shear stress,[11] cyclic tension,[18,19]

[1]Demirci Bio-Acoustic-MEMS in Medicine (BAMM) Laboratory, Department of Medicine, Center for Biomedical Engineering, Brigham and Women's Hospital, Harvard Medical School, Boston, Massachusetts.
[2]Harvard-MIT Health Sciences and Technology, Cambridge, Massachusetts.
*These authors contributed equally to this work.

and combined stimulation),[20] electrical stimulation,[21] and bioprinting.[22–27] Quantification of cellular alignment is necessary to validate the effectiveness of these approaches and the engineered microenvironment. Therefore, quantification of cellular alignment and organization with a rapid, accurate, and adaptable method would be significant in assessing the organization of cells in engineered tissues and biomaterials.

Quantification of cellular alignment is generally performed on microscope images obtained with imaging techniques, including phase-contrast (e.g., cell monolayers), bright-field (e.g., histological sections), and fluorescent microscopy (e.g., immunostaining and confocal microscopy). Cellular alignment evaluation generally involves one or combination of the following processes: (1) identification of cell outlines and determination of the relative orientations of the cells, (2) identification of elongation and cumulative orientation of the cellular nuclei, and (3) identification and assessment of orientation of cytoskeletal components (e.g., actin, vimentin, and tubulin filaments). Therefore, a method developed for the assessment of cellular alignment should be adaptable to recognize the type of information available in the images and to assign a score in close agreement with manual quantification in an automated manner.

Although quantification of cellular alignment by measuring its physical consequences (e.g., mechanical anisotropy or polarization of infrared light) have been achieved before,[28] this is generally performed in the laboratories primarily by analyzing microscope images using manual measurements[29,30] or automated methods.[11,31,32] Although manual measurement is reliable,[33] it suffers from several limitations: (i) it is tedious and time consuming, (ii) the processing efficiency is low especially when multiple images with hundreds of cells are needed to be processed, and (iii) it has interoperator variability. Various automated image-processing methods have also been employed to quantify cell alignment from images, a majority of which are based on the Fast Fourier Transform-Radial Sum (FFTRS)[31] and gradient based[11,32] methods. Here, FFTRS follows the FFT-based radial sum ap-

proach described in reference.[34] However, these automated methods were not specifically developed for recognizing and quantifying cellular alignment, and hence display complexities as listed above. Specifically, being an indirect measure of cellular orientation, FFT-based methods yield low alignment scores even on images having perfect alignment of cells since the frequency spectrum of an image has frequency components other than in the direction of cell orientation. Therefore, these methods do not necessarily recognize the type of information available (i.e., cellular outline, nucleus, or cytoskeleton) in the microscope image and produce a result accordingly. To address the aforementioned challenges associated with the currently available automated techniques, we propose a rapid, accurate, and adaptable method (binarization-based extraction of alignment score [BEAS]) to quantify cellular alignment from microscope images obtained with various methods: phase-contrast, bright-field, and immunofluorescent microscopy. BEAS method works with unlabelled cells, immunolabeled cells, and cells displaying bipolar morphology (e.g., SMCs, cardiomyocytes, and neurons). We show here that BEAS cellular alignment quantification method provides a rapid, accurate, and adaptable alternative to currently available automated methods with results that more closely agree with manual quantification results.

Methods

Images

To compare BEAS method with existing methods, we used test images with manually measured score for cell alignment. Test images (Fig. 1a and Fig. 2a) were prepared using Adobe Flash (Adobe Systems Incorporated, San Jose, CA). The first test image (Fig. 1a) examined the signal that each method produced from a set of perfectly aligned objects (all the objects aligned in the same direction with orientations of 90°). It consisted of an array of solid black ellipses mimicking bipolar type cells or cellular nuclei, each 75 pixels tall and 25 pixels wide (approximating cell size in 10× images). The

FIG. 1. Performance of existing automated methods for quantifying a test image composed of representative cells (ellipsoid objects). The orientation distribution of an array of ellipses **(a)**, all vertically oriented, was evaluated using the FFT, gradient, and BEAS methods **(b)**. Angles are counter-clockwise from horizontal. While the FFT method gave a peak angle (89.57°) close to the correct value of 90°, its background signal is nearly as high as the peak (peak/mean = 1.24). This results in an alignment score of only 0.0443 (0–1 scale), despite the fact that the ellipses are perfectly aligned. The gradient method gave an essentially correct peak angle (89.99°), and it had a much lower background signal. However, because it measures edge orientation rather than object orientation, it has signal from the parts of the ellipse edges that are not aligned with the whole ellipses. It gave an alignment score of 0.6796, a marked improvement over FFT, but still far from the correct value of 1. BEAS method gave a peak angle of 89.30° and an alignment score of 0.9998. Black = FTT, blue = gradient, red = BEAS. BEAS, binarization-based extraction of alignment score; FFT, fast Fourier transform. Color images available online at www.liebertonline.com/tec
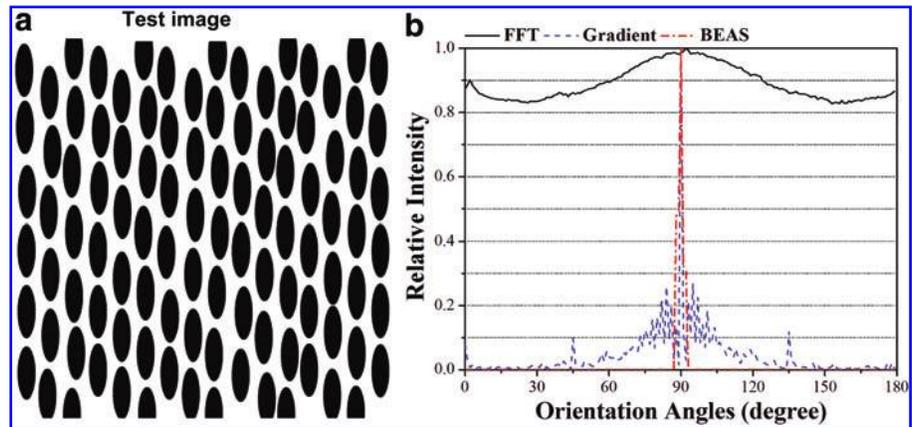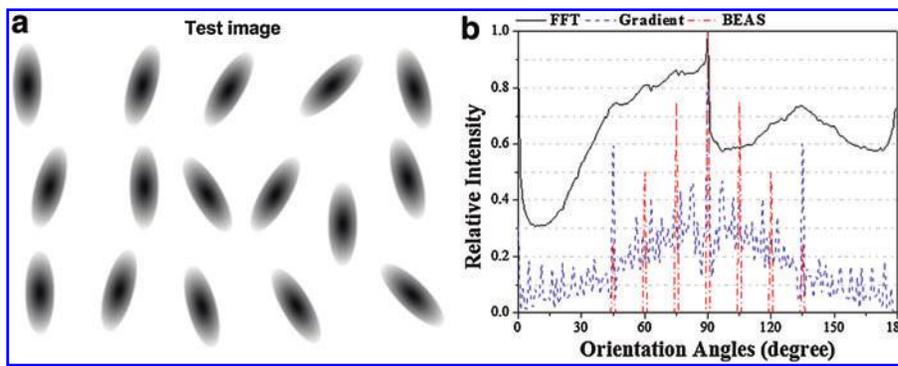
FIG. 2. BEAS method accurately measures orientation distribution for images with objects aligned in multiple directions. **(a)** A test image consisting of 16 ellipses (aspect ratio = 4), oriented as follows: 1 at 45°, 2 at 60°, 3 at 75°, 4 at 90°, 3 at 105°, 2 at 120°, and 1 at 135°. The orientation distribution should thus have a 1:2:3:4:3:2:1 ratio between those angles, and no signal anywhere else. **(b)** Orientation distributions as determined by FFT (black line), gradient (blue line), and BEAS method (red line). Angles are counter-clockwise from horizontal. Although the true orientation distribution was highly symmetrical, the FFT method gave a highly asymmetrical distribution, with a large signal at all angles, and no distinct peaks corresponding to the ellipses at angles other than 90°. The FFT method also gave a strong peak orthogonal to the highest peak. The gradient method correctly gave a reasonably symmetrical distribution, but it had high peaks at 45° and 135°, and many smaller peaks distributed throughout the set of possible angles. BEAS method gave peaks only at the angles at which ellipses were oriented, with no background signal. Although the heights of the peaks do not correspond to the number of ellipses at each orientation due to the cut-offs for each bin, the areas under the peaks have a ratio of 1.00:1.99:2.99:3.81:2.98:1.99:1.00, very close to the correct ratio of 1:2:3:4:3:2:1. The alignment score calculated from this distribution is 0.6981, very close to the correct value of 0.6998. Color images available online at www.liebertonline.com/tec

ellipses were arranged into columns, with 7 pixels of white space between neighboring ellipses. Each column was vertically offset 25 pixels down from its left neighbor. Each ellipse was then randomly moved upward to five pixels left or right and up to five pixels up or down. The second test image examined each method's ability to discern orientation distribution for less sharp objects (i.e., with blurred boundary, Fig. 2a). An image consisting of 16 ellipses (200 × 67 pixels), each with a black center that fades out to light gray at the edges, was prepared. The ellipses had orientations with respect to horizontal direction of 45° (1), 60° (2), 75° (3), 90° (4), 105° (3), 120° (2), and 135° (1).

Cell images from our laboratory were taken of printed primary SMCs isolated from rodent (Sprague-Dawley rat, female, 250–300 g) bladder tissue, sacrificed under the approval of Institutional Animal Care and Use Committee. Other cell images were taken from published literature as the source of each image is noted in Supplementary Table S1 (Supplementary Data are available online at www.liebertonline.com/tec). Selected images cover multiple imaging modalities (phase-contrast, bright-field, and fluorescence) and multiple bipolar cell types. Cell types included SMC, endothelial cells, fibroblasts, skeletal muscle cells, and astrocytes.

Overview of alignment quantification process

Methods to quantify cell alignment can be broken down into three basic steps: (i) image transformation, in which the microscopic image is converted to a form (e.g., binary image) from which orientation information (e.g., orientation angle of individual objects, object size) can be extracted, (ii) cell orientation extraction, in which an orientation distribution is generated from the transformed image, and (iii) cell alignment score representing the degree of cell–cell alignment is calculated from the orientation distribution.

The orientation distribution is a periodic function $f(\theta)$ with a period of π radians such that for any angle $\theta \in [0, \pi)$, $f(\theta)$ represents the relative contribution of objects oriented in the

θ direction to the image. $\theta = 0$ represents the x-axis, and θ increases in the counter-clockwise direction. Orientation distributions are graphed with angles (degrees) and scaled such that their maximum value is 1.

Preprocessing

Images were preprocessed using a despeckle filter followed by a (Gaussian) Band-pass filter (see Supplemental Materials) using the public domain NIH ImageJ program (developed at the U.S. National Institutes of Health and available at http://rsb.info.nih.gov/nih-image/).[35] The despeckle filter removes single-pixel noise, and the band-pass filter corrects for uneven illumination by removing high-frequency components from the image, and mitigates the effect of fibers, noise, and/or other features than cells by removing low frequency components (blurring the image).

Binarization

Binary images were generated by Sauvola's local thresholding algorithm (using the Auto Local Threshold plug-in in ImageJ software[35]) with a user-defined radius to each preprocessed image[36] (see Supplemental Materials). Local thresholding was used because global thresholds performed poorly on our images (Fig. 3 and Fig. S1), since global thresholding uses a single threshold value for the whole image. Global thresholding may bring more errors to the binary image due to uneven image features varying across the image (e.g., brightness and background intensity) and that would cause misdetection of background as cells.

This challenge can be addressed by using multiple thresholds for local areas of the image. Each contiguous block of pixels less than the threshold brightness was then treated as an object (for fluorescence images, pixels greater than the threshold brightness were used). All holes (regions of "background" completely enclosed by cells) in detected objects were filled, followed by the "open" operation (erosion and dilation, which removes features of single-pixel width) using the Open and Fill Holes functions in ImageJ

FIG. 3. The steps of BEAS method for quantify cell alignment are illustrated using an image of cultured smooth muscle cells. **(a)** Original image. **(b)** The image is preprocessed, by applying a despeckle filter to reduce noise (the value of each pixel is replaced by the median of the 3×3 square centered around it), followed by a band-pass filter to filter out extracellular fibers and debris and correct for uneven lighting. **(c)** The image is then binarized using Sauvola's adaptive thresholding algorithm.[36] **(d)** Open (remove one-pixel thin structures) and Fill Holes operations are applied to the binary image. **(e)** The angle of orientation of each object in the binary image is calculated, and the objects are weighted by area to produce an orientation distribution. Scale bar: 100 µm.
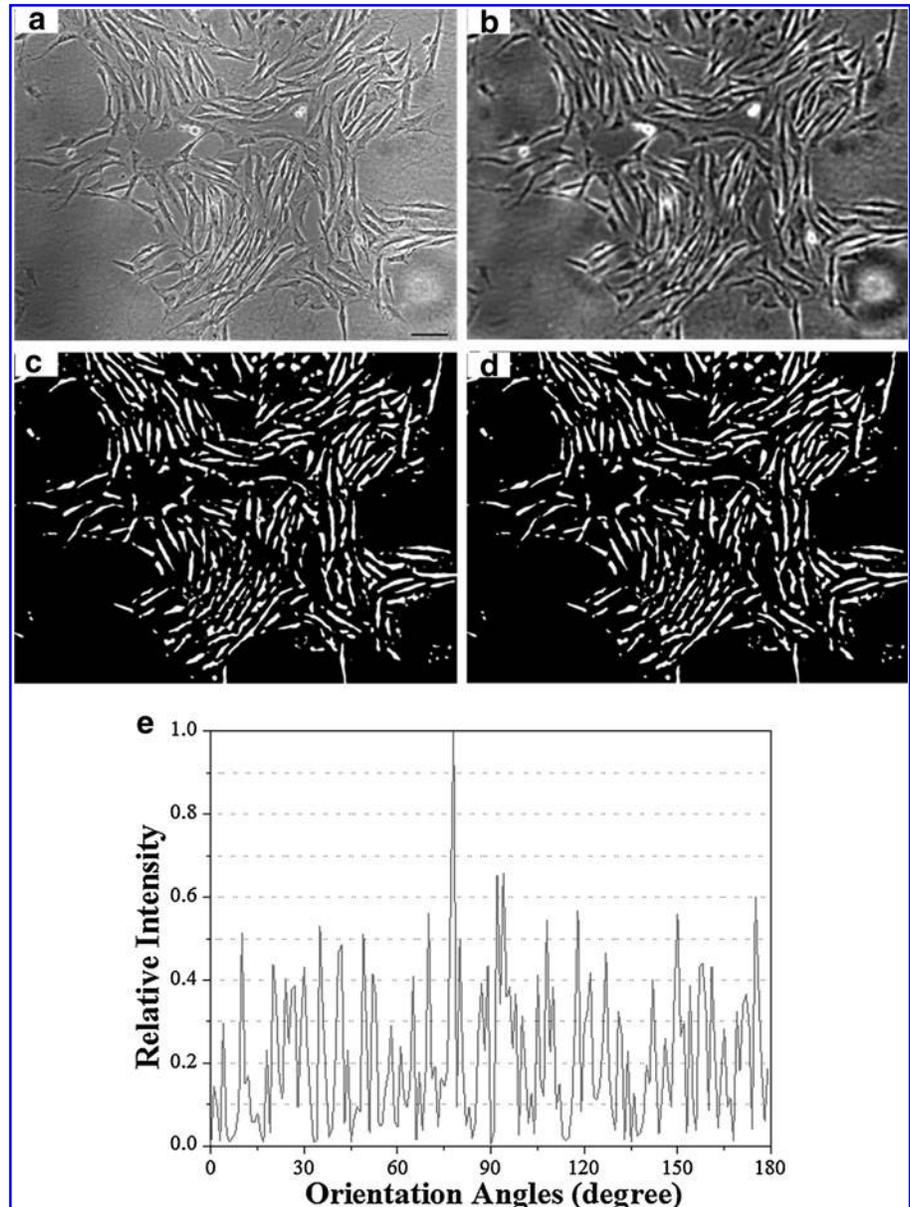
software.[35] The remaining objects were considered to be cells, and their size and orientation were then calculated. These operations were implemented MATLAB (2008a, The MathWorks, Natick, MA).

Determination of orientation distribution

Orientation distribution, defined as the amount of the objects that are oriented in each direction, was determined from the size T and orientation $\varphi \in [0, \pi)$ of each object (e.g., cells) in the binary image, according to

$$f(\theta) = \sum_n T_n * \delta(\theta - \varphi_n) \quad (1)$$

The distribution f is repeated with period π. T_n was defined as the area of each cell for the area-weighted distribution, and the length of each cell for the length-weighted distribution.

Automated measurement of cell properties in the image

Cell properties in the image such as the area, center location, and orientation were calculated for each cell as these parameters are defined as follows. The area was taken to be the number of pixels each cell contained. The center of each cell was determined by taking the average x and y coordinates for all the pixels of cell area. To find cell orientation, a line was drawn through the center, and the orientation that gave the minimized sum of the squares of each pixel's shortest distance to the line was used (Supplementary Fig. S2), as follows.

$$\min_{\varphi=[0,\pi)} \left(D(\varphi) = \sum_n d_n \right) \quad (2)$$

Cell length was considered to be the length of the major axis of the best-fit ellipse for each cell.

Quantification of alignment and overall orientation

Functions performing quantification of alignment and extracting overall orientation are implemented in MATLAB (2008a, The MathWorks) as follows: For each angle θ, the degree $A(\theta)$ to which the cells were aligned in the θ direction was calculated by taking the average, weighted by cell size, of the cosine of twice each cell's angle relative to θ:

$$A(\theta) = \frac{\sum_n T_n \cos(2(\varphi - \theta))}{\sum_n T_n} \qquad (3)$$

The overall direction of alignment θ^* was defined to be the value of θ that maximized $A(\theta)$. The degree of cell–cell alignment A^* was defined to be $A(\theta^*)$. A weighted average was used because it is not possible to guarantee that every recognized region is a cell, and very small objects are more likely to represent false positives than cell-sized objects. Further, if two cells are recognized as a single object, that object will be approximately twice as large as a single cell; weighting by size means that an object that represents two cells is given twice the weight of an object that represents only one. This means that this method is a function of cell density. Although it cannot fully characterize a grown bundle of cells, it can monitor them as the tissue construct matures.

Using $\cos(2(\varphi - \theta))$ to quantify alignment has several advantages. It is a continuous, even periodic function that helps prevent artifacts; further, it is a good representation of the physical consequences of alignment (see Supplementary Materials). It also means that A^* varies along [0, 1], where 0 corresponds to randomly oriented cells, and 1 corresponds to perfect alignment. For proper functioning of bladder smooth muscle, the degree to which the cells are aligned to each other, rather than to an externally defined direction, is more important for tissue function, so A^* was used as the metric for cell alignment in a given image. It should be noted, however, that if alignment with an externally defined direction α is preferred for a particular application, $A(\alpha)$ can be used as the alignment score.

Comparison of orientation distributions

Automated methods of generating orientation distributions were evaluated according to two separate metrics as described below. Each method's ability to determine accurate alignment scores was assessed by the degree to which A^* scores from manually measured orientation distributions predicted A^* values from that method (determined using r^2). r^2 was used because it is not sensitive to scores that differ only by a constant or a scale factor. The FFTRS and gradient methods necessarily give lower A^* scores than BEAS method and manual measurement do (see Supplementary Materials), but this does not preclude the possibility that their A^* scores could be scaled to match those of manual measurement.

Manual measurement and current automated methods

Four researchers manually analyzed the cellular alignment independently using the line drawing function using ImageJ to obtain an angle for each object. For each image, a line segment was manually drawn end-to-end through each cell. The size of each cell was taken to be the length of the line segment drawn through the cell, and its orientation was taken to be the orientation angle of the line segment relative to the x-axis. The data for each object were transferred to a spreadsheet, and the average alignment was calculated. The results from four manual counters were averaged. Two current automated methods (e.g., gradient method and FFTRS method) were compared with BEAS method in this study. In the gradient method of cell alignment, the gradient of the image is calculated at each point using the Sobel operator.[37] The orientation distribution is determined by the gradient direction at each point, with points weighted by the gradient magnitude. In the FFTRS method, first the FFT of the image is calculated, and then shifted so that the DC component (constant component) is in the center. A circle is then drawn tangent to the boundaries of the transformed image, and the contribution of cells oriented at each angle is equated to the sum of the intensity magnitude along the circle diameter at that angle, using ImageJ software.[34,35]

Statistical analysis

Cellular orientation scores obtained from BEAS, FFTRS, and Gradient-based methods were statistically compared with the scores obtained from the Manual method by utilizing paired t-test. A variety of microscopic images (i.e., phase-contrast, bright-field, and fluorescent microscopy) were used to validate the methods ($n = 15$). Linear regression with least squares method was used to apply a linear fit for the data to observe the relation between the BEAS, FFTRS, Gradient based methods, and the Manual Method. Statistical significance threshold was set at 0.01 ($p < 0.01$). Error bars in the figures represent standard deviation.

Results

Comparison of FFTRS, gradient, and BEAS methods using test images

We tested FFTRS, gradient, and BEAS methods to determine cell orientation distribution using prepared test images with known distributions. The true orientation distribution in the first test image (Fig. 1a) was a signal at 90° and no signal at other angles, with $\theta^* = 90$ and $A^* = 1$. The gradient method gave a θ^* value of 89.99°; the other two methods gave less accurate θ^* values (0.0443 for FFTRS method and 0.6796 for gradient method), though both were within one degree of 90°. Only BEAS method gave accurate A^* values (0.9998 for both the length-weighted and area-weighted variants). BEAS method gave an orientation distribution consisting of a single sharp peak, with non-zero signal only in the range of 87°–93°. The gradient method gave a broad peak at 90°, with small but nonzero background signal throughout. The FFTRS method gave large background signal throughout, with a strong, broad peak at 90° and a small peak at 0°.

Next, we tested each method's ability to discern orientation distribution for less sharp objects (Fig. 2). An image consisting of 16 ellipses (200 × 67 pixels), each with a black center that fades out to light grey at the edges was prepared. The ellipses had orientations of 45° (1), 60° (2), 75° (3), 90° (4), 105° (3), 120° (2), and 135° (1); the true value of θ^* was 90° and the true value of A^* was 0.6998. Although the true orientation distribution was symmetrical about 90°, the FFTRS

method gave a highly asymmetric distribution. The gradient method and BEAS method gave more symmetrical distributions. The gradient method had a large number of small peaks (noise signal), plus large peaks at 45°, 90°, and 135°. BEAS method gave sharp peaks at the angles at which the ellipses were oriented, and the areas under the peaks were close to the correct ratio for the ellipses' orientations.

Quantification of cell orientation and cell–cell alignment

BEAS method was tested using 15 bipolar cell images (described in Supplementary Materials Table S1), containing a variety of cell types and imaging modalities. Some of the images were adapted from the published literature (see Table S1), and some were produced in our lab. Each image was processed as described to give a binary image (illustrated in Fig. 3a–d; each image in each major step is shown in Fig. S3). The orientation distribution was extracted from each binary image as described (distributions are graphed in Fig. S3), and from each original image by the FFTRS and gradient methods. The cell orientations in each image were also manually measured by three students. The different orientation distributions produced for each image were compared (Table S2).

The adaptability of the BEAS method was validated by conducting the cellular alignment analysis a variety of microscope images: phase-contrast, bright-field, fluorescent microscopy, and confocal imaging (Supplementary Fig. S3, Fig. 3, Fig. 4, Fig. S4). BEAS method successfully adapted to each image type by consistently producing comparable results with the manual method.

BEAS method resulted in statistically comparable ($p > 0.1$) alignment scores with the manual method for the 15 different images analyzed, whereas the FFTRS and gradient-based method scores were significantly different ($p < 0.01$) from the manual method results (Fig. 5a). Further, alignment scores obtained from BEAS method displayed a linear correlation with the results obtained via manual method (coefficient of determination [R^2]: 0.92) (Fig. 5b). The gradient method values were consistently lower than manual results with a correlation of $R^2 = 0.74$. Similarly, the FFTRS method scores were lower than all methods, and these scores did not correlate with scores produced manually ($R^2 = 0.04$, Fig. 5b).

Discussion

The results presented here illustrated the comparison between orientation results obtained from manual measurement, BEAS, the FFTRS, and gradient based methods. In the gradient method, each cell contributes to the score in almost all directions (though unequally), whereas in BEAS method and manual measurement, each cell contributes to the score only in its putative direction or orientation. Similarly, FFTRS method possesses significant signal components in almost all directions since a certain cell image, even comprising cells perfectly aligned in one direction, cannot be represented by only one frequency component. This effect might especially be significant in determining cell orientation rather than fiber as perfectly aligned fiber images would be more similar to a cosine-like image (having only one frequency component), which might make them more suitable to be processed with FFTRS method.

This difference can be clearly seen in Figure 1, which shows the orientation distributions that each method pro-
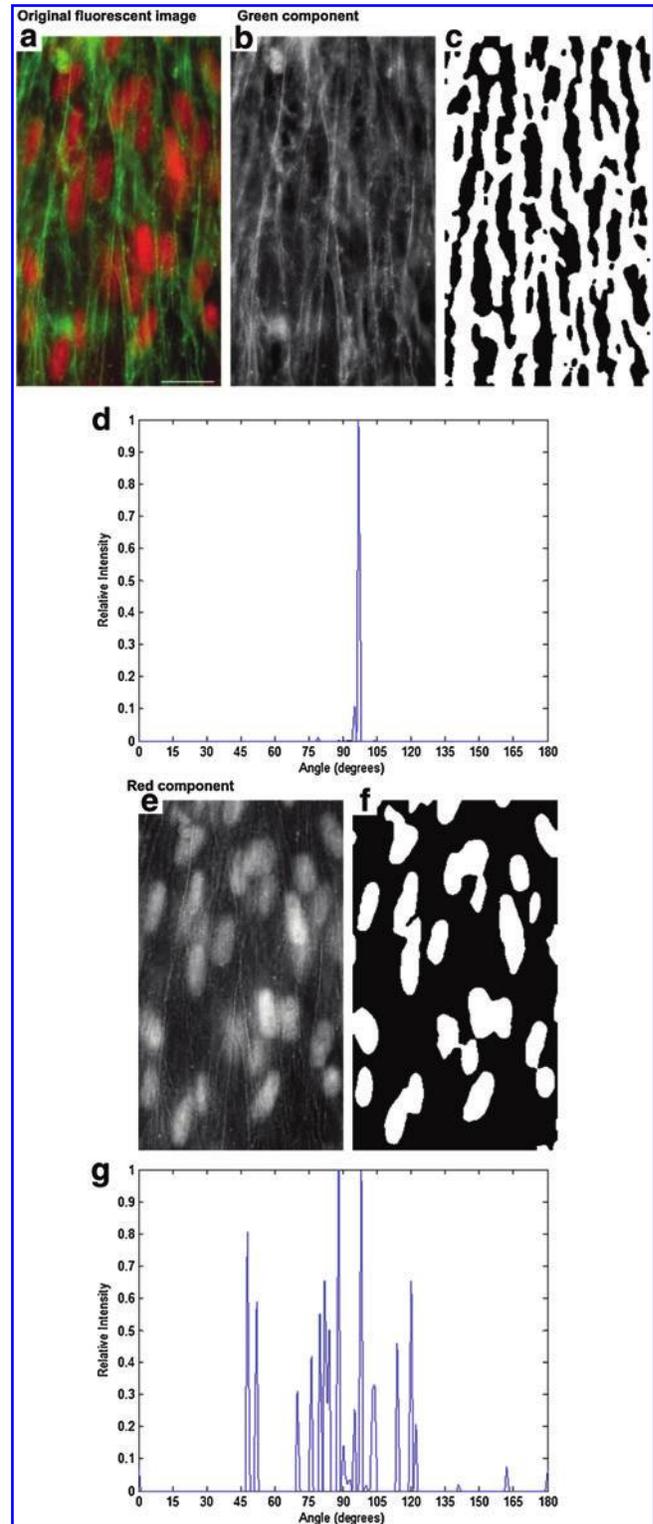
FIG. 4. Quantification of the cytoskeletal and nuclear alignment of cells stained with fluorescent dyes. **(a)** The cells are located on a biomaterial surface and display a complex three-dimensional distribution. The alignment quantification method presented here can quantify the cytoskeletal **(b-d)** and nuclear **(e-g)** alignment of the cells. (**a**: adapted from[31]). Scale bar: 20 µm. Color images available online at www.liebertonline.com/tec
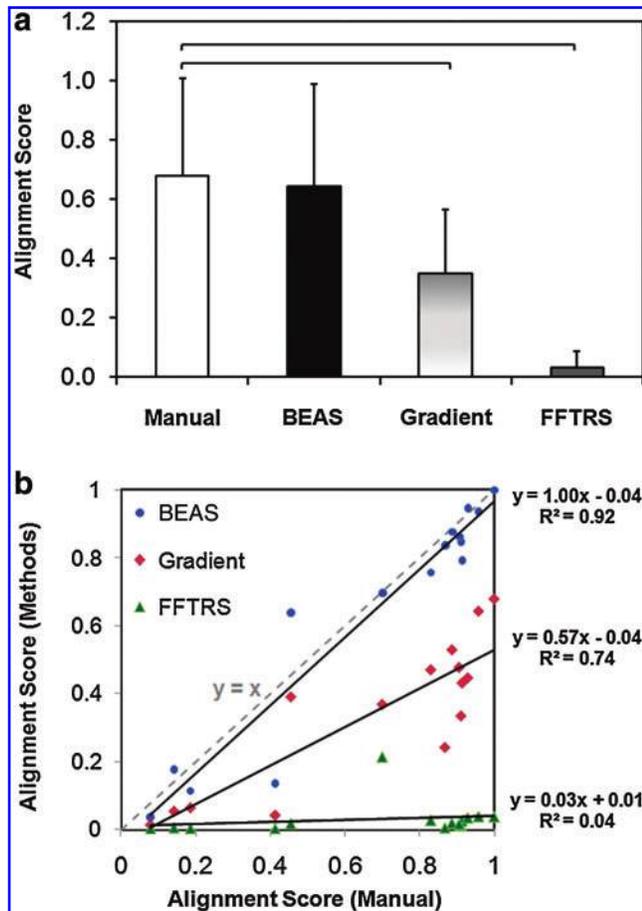
FIG. 5. Comparison of scores from manual measurement with BEAS, Gradient, and FFTRS methods. **(a)** Alignment score of the analyzed images did not display a statistically significant difference between the manual scoring and the BEAS method developed in this study. On the other hand, the Gradient and FFTRS-based methods displayed significant difference compared to the manual scoring method. Brackets indicate statisticaly significant difference ($p < 0.01$, paired t-test) between the groups ($n = 15$ per group). **(b)** Linear regression between the manual alignment scoring and the BEAS, Gradient, and FFTRS methods. BEAS method displayed the highest level of correlation ($y = x - 0.04$) with the manual scoring method with the highest regression score ($R^2 = 0.92$). Even though the Gradient and FFTRS-based scoring methods displayed agreement with the manual scoring, their correlation and regression scores were significantly lower than the BEAS method. FFTRS, fast Fourier transform-radial sum. Color images available online at www.liebertonline.com/tec

duces for an image where all objects are oriented in one direction. The difficulty posed by each cell contributing signal in all angles is apparent in Figure 2, where BEAS method gives an orientation distribution very close to the manual scoring, whereas the FFTRS and gradient methods do not.

BEAS method produced alignment scores that strongly predict those produced manually (Table S2, Fig. 5) and orientation distributions that are, on average, as similar to manually measured distributions as the manually measured distributions are to each other (Fig. 5a). Linear regression (Fig. 5b) showed that BEAS method more accurately pre-

dicted the results of manual measurement of cell–cell alignment than the gradient method, and the FFTRS method did not appear to predict at all. This result indicated that the alignment scores that the FFTRS and gradient method gave are not simply off by a scale factor. They produced distributions that reflect both cell–cell alignment and other unknown factors, and isolating the alignment information from the other information present is a complex task that likely must be done on a case-by-case basis. The difference in the alignment results on Table S2 between the manual and BEAS is mainly due to the fact that the cells in the images cannot be easily differentiated from the background. In these images, some of the background was identified as cells and some of the cells were not fully captured by the code, and assessed as background. Potential sources of this difference are confluence of cells, and lack of contrast between the cells and the background in the images. By improving the image quality, the outcomes can be significantly improved to allow a better agreement between the manual and software analysis.

Despite the high accuracy for measuring alignment and orientation, our method does not precisely identify all individual cells. Rather, the binary images it produces disregard some cells, count some artifacts that are not associated with cells, and merge some cells into single objects. Size-based weighting enables it to give accurate results despite these errors. The noncell objects mistakenly registered as cells are, for the most part, smaller than cells. As a result, their contribution to the overall orientation distribution is small, particularly when the distribution is weighted by object area. When the number of cells in an image is large, the failure to pick up a few poorly illuminated cells is unlikely to significantly alter the overall distribution. If two cell areas are fused into one, the resulting object will have approximately twice the area of a single cell, and will consequently be weighted as two cells. The image recognition aspect of the code can be modified to perform orientation per cell and number of objects processed. Currently, the program provides the overall average cell orientation of a sample. Further, for cell types whose primary function is mechanical, the quantity of intracellular cytoskeletal components (e.g., f-actin filaments inside the cells) is generally more important than cell number, and an area-weighted distribution more accurately reflects the distribution of these elements (Fig. 4).[7,38] If multiple images in a time series are compared, cells can divide without affecting the orientation distribution, because each daughter cell will initially have half the area of the mother cell. A length-weighted distribution, meanwhile, more closely resembles the way in which manually measured distributions are calculated, and consequently serves as a direct comparison between manual and automated results.

BEAS method was able to determine orientation distribution and cell–cell alignment in images of multiple cell types using multiple imaging modalities. It was able to work with these different images because of key features that they have in common: the objects of interest are contiguous regions either increased (fluorescence) or decreased (bright field and phase contrast) luminosity, they are much wider than fragments not of interest, and they have a bipolar morphology.

BEAS method calculates cell orientation relative to a rectangular coordinate system without regarding to each cell's position. The scoring method we used assumes that uniaxial alignment (all cells orienting in a single direction)

is to be measured. If another form of alignment (e.g., circumferential alignment of vascular SMCs in blood vessels) is needed, BEAS method can be used to produce an orientation distribution, which can then be scored. Besides, in BEAS method the code picks the two far most distant locations of the object to draw a line for alignment. As long as the object shape is not a perfect circle (Fig. S4), the code will be able to process the image and determine the orientation of the object.

Conclusions

In this study, we developed a BEAS method for quantifying the alignment of cells in biomaterials and tissue-engineered constructs. The results indicated that BEAS alignment scores agreed closely and correlated with the manual method results, indicating that this method is rapid, accurate, and adaptable. Therefore, BEAS method has the potential to find widespread applications in accurately and rapidly quantifying cellular alignment in biomaterial development and tissue engineering research.

Acknowledgments

Disclosure Statement

No competing financial interests exist.

Author Contributions

F.X. and U.D. suggested the idea; T.B., E.F., and F.X. developed the program; T.B., F.X., E.F., U.A.G, and U.D. performed image analyses; F.X., T.B., E.H., U.A.G., and U.D. wrote the article.

References

1. Geckil, H., Xu, F., Moon, S., and Demirci, U. Mimicking the extracellular matrix: engineering a controlled three-dimensional cell microenvironment. NanoMed **5,** 469, 2010.
2. Wang, W., Itoh, S., Konno, K., Kikkawa, T., Ichinose, S., Sakai, K., *et al.* Effects of Schwann cell alignment along the oriented electrospun chitosan nanofibers on nerve regeneration. J Biomed Mater Res **91,** 994, 2009.
3. Bozkurt, A., Deumens, R., Beckmann, C., Olde Damink, L., Schugner, F., Heschel, I., *et al. In vitro* cell alignment obtained with a Schwann cell enriched microstructured nerve guide with longitudinal guidance channels. Biomaterials **30,** 169, 2009.
4. Fung, Y.C. Biomechanics: Mechanical Properties of Living Tissues. New York: Springer-Verlag, 1993.
5. Black, L.D., 3rd, Meyers, J.D., Weinbaum, J.S., Shvelidze, Y.A., and Tranquillo, R.T. Cell-induced alignment augments twitch force in fibrin gel-based engineered myocardium via gap junction modification. Tissue Eng **15,** 3099, 2009.
6. Wolinsky, H., and Glagov, S. Structural basis for the static mechanical properties of the aortic media. Circ Res **14,** 400, 1964.
7. Gurkan, U.A., Cheng, X.G., Kishore, V., Uquillas, J.A., and Akkus, O. Comparison of morphology, orientation, and migration of tendon derived fibroblasts and bone marrow stromal cells on electrochemically aligned collagen constructs. J Biomed Mater Res Part A **94A,**1070, 2010.
8. Kapoor, A., Caporali, E.H.G., Kenis, P.J.A., and Stewart, M.C. Microtopographically patterned surfaces promote the alignment of tenocytes and extracellular collagen. Acta Biomater **6,** 2580, 2010.
9. Cha, J.M., Park, S.N., Noh, S.H., and Suh, H. Time-dependent modulation of alignment and differentiation of smooth muscle cells seeded on a porous substrate undergoing cyclic mechanical strain. Artif Organs **30,** 250, 2006.
10. Ritchie, A.C., Wijaya, S., Ong, W.F., Zhong, S.P., and Chian, K.S. Dependence of alignment direction on magnitude of strain in esophageal smooth muscle cells. Biotechnol Bioeng **102,** 1703, 2009.
11. Lee, A.A., Graham, D.A., Dela Cruz, S., Ratcliffe, A., and Karlon, W.J. Fluid shear stress-induced alignment of cultured vascular smooth muscle cells. J Biomech Eng **124,** 37, 2002.
12. Mummery, C.L., Davis, R.P., and Krieger, J.E. Challenges in using stem cells for cardiac repair. Sci Transl Med **2,** 27ps17, 2010.
13. Tranquillo, R.T., Girton, T.S., Bromberek, B.A., Triebes, T.G., and Mooradian, D.L. Magnetically orientated tissue-equivalent tubes: application to a circumferentially orientated media-equivalent. Biomaterials **17,** 349, 1996.
14. Thomopoulos, S., Das, R., Birman, V., Smith, L., Ku, K., Elson, E., *et al.* Fibrocartilage tissue engineering: the role of the stress environment on cell morphology and matrix expression. Tissue Eng Part A **17,** 1039, 2011.
15. Freegard, T.J. The physical basis of transparency of the normal cornea. Eye **11,** 465, 1997.
16. Fernandez, J.G., Mills, C.A., and Samitier, J. Complex microstructured 3D surfaces using chitosan biopolymer. Small **5,** 614, 2009.
17. Barry, R.A., Shepherd, R.F., Hanson, J.N., Nuzzo, R.G., Wiltzius, P., and Lewis, J.A. Direct-write assembly of 3D hydrogel scaffolds for guided cell growth. Adv Mater **21,** 1, 2009.
18. Silbert, O., Wang, Y., Maciejewski, B.S., Lee, H.S., Shaw, S.K., and Sanchez-Esteban, J. Roles of RhoA and Rac1 on actin remodeling and cell alignment and differentiation in fetal type II epithelial cells exposed to cyclic mechanical stretch. Exp Lung Res **34,** 663, 2008.
19. Standley, P.R., Cammarata, A., Nolan, B.P., Purgason, C.T., and Stanley, M.A. Cyclic stretch induces vascular smooth muscle cell alignment via NO signaling. Am J Physiol **283,** H1907, 2002.
20. Houtchens, G.R., Foster, M.D., Desai, T.A., Morgan, E.F., and Wong, J.Y. Combined effects of microtopography and cyclic strain on vascular smooth muscle cell orientation. J Biomech **41,** 762, 2008.
21. Rajnicek, A.M., Foubister, L.E., and McCaig, C.D. Alignment of corneal and lens epithelial cells by co-operative effects of

substratum topography and DC electric fields. Biomaterials **29,** 2082, 2008.

22. Tasoglu, S., Kaynak, G., Szeri, A.J., Demirci, U., and Muradoglu, M. Impact of a compound droplet on a flat surface: A model for single cell epitaxy. Physic of Fluidics **22,** 18, 2010.

23. Song, Y.S., Adler, D., Xu, F., *et al.* Proceedings of the National Academy of Sciences of the United States of America **107,** 4596, 2010.

24. Xu, F., Moon, S., Emre, A.E., Turali, E.S., Song, Y.S., Hacking, A., Nagatomi, J., and Demirci, U. A Droplet based building block approach for bladder smooth muscle cell (SMC) proliferation. Biofabrication **2,** 2010. doi: 10.1088/1758-5082/2/1/014105.

25. Moon, S., Hasan, S.K., Song, Y.S., Keles, H.O., Manzur, F., Mikkilineni, S., Hong, J.W., Nagatomi, J., Haeggstrom, E., Khademhosseini, A., and Demirci, U. Layer by layer 3D tissue epitaxy by cell laden hydrogel droplets. Tissue Eng C **16,** 157, 2010.

26. Moon, S., Kim, Y., Dong, L., Lombardi, M., Haeggstrom E., Jensen, R.V., Hsiao, L., and Demirci, U. Drop-on-demand single cell isolation and total RNA analysis. PLoS ONE **6,** e17455, 2011.

27. Xu, F., Sridharan, B., Wang, S., Gurkan, U.A., Syverud, B., and Demirci, U. Embryonic Stem Cell Printing for Controllable Uniform Sized Embryoid Body Formation. Biomicrofluidics, 2011.

28. Wang, J.H., Jia, F., Gilbert, T.W., and Woo, S.L. Cell orientation determines the alignment of cell-produced collagenous matrix. J Biomech **36,** 97, 2003.

29. Knapp, D.M., Helou, E.F., and Tranquillo, R.T. A fibrin or collagen gel assay for tissue cell chemotaxis: assessment of fibroblast chemotaxis to GRGDSP. Exp Cell Res **247,** 543, 1999.

30. Houtchensa, G.R., Foster, M.D., Desai, T.A., Morgan, E.F., and Wong, J.Y. Combined effects of microtopography and cyclic strain on vascular smooth muscle cell orientation. J Biomech **41,** 762, 2008.

31. Ng, C.P., Hinz, B., and Swartz, M.A. Interstitial fluid flow induces myofibroblast differentiation and collagen alignment *in vitro*. J Cell Sci **118,** 4731, 2005.

32. Karlon, W.J., Hsu, P.P., Li, S., Chien, S., McCulloch, A.D., and Omens, J.H. Measurement of orientation and distribution of cellular alignment and cytoskeletal organization. Ann Biomed Eng **27,** 712, 1999.

33. Alyassin, M.A., Moon, S., Keles, H.O., Manzur, F., Lin, R.L., Haeggstrom, E., *et al.* Rapid automated cell quantification on HIV microfluidic devices. Lab Chip **9,** 3364, 2009.

34. Alexander, J.K., Fuss, B., and Colello, R.J. Electric field-induced astrocyte alignment directs neurite outgrowth. Neuron Glia Biol **2,** 93, 2006.

35. Rasband, W.S. ImageJ. http://rsbinfonihgov/ij/, National Institutes of Health, Bethesda, MD, 1997–2009.

36. Sauvola, J., and Pietikainen, M. Adaptive document image binarization. Pattern Recognit **33,** 225, 2000.

37. Engel, K., Hadwiger, M., Kniss, J., Rezk-Salama, C., and Weiskopf, D. Real-Time Volume Graphics. Natick, MA: A.K. Peters Ltd., 2006.

38. Hashi, C.K., Zhu, Y.Q., Yang, G.Y., Young, W.L., Hsiao, B.S., Wang, K., *et al.* Antithrombogenic property of bone marrow mesenchymal stem cells in nanofibrous vascular grafts. Proc Natl Acad Sci USA **104,** 11915, 2007.

Address correspondence to:
Utkan Demirci, Ph.D.
65 Landsdowne Street, PRB 267
Cambridge, MA 02139

E-mail: udemirci@rics.bwh.harvard.edu

Supplemental Materials

Automated Quantification of Cell-Cell Alignment from Microscopic Images for Tissue Engineering Applications

Feng Xu [a*], Turker Beyazoglu [a*], Evan Hefner [a], Umut A. Gurkan [a], Utkan Demirci [a,b#]

[a] *Demirci Bio-Acoustic-MEMS in Medicine (BAMM) Laboratory, Center for Biomedical Engineering, Department of Medicine, Brigham and Women's Hospital, Harvard Medical School, Boston, MA, USA*
[b] *Harvard-MIT Health Sciences and Technology, Cambridge, MA, USA.*
[*] *Authors contributed equally*
[#] *Corresponding author: udemirci@rics.bwh.harvard.edu*

S.1. Implementation of Binarization based Extraction of Alignment Score (BEAS) Method

The sequence of BEAS method is as follows:

i. Despeckle Filter
ii. Gaussian Band-pass Filter
iii. Auto Local thresholding
iv. Fill holes and Open
v. Extraction of orientation angle of the objects from the binary image

The first 4 operations are performed using the image processing software ImageJ (Rasband, W.S., ImageJ, U.S. National Institutes of Health, Bethesda, Maryland, USA, http://rsb.info.nih.gov/ij/, 1997-2009). ImageJ can recognize various file formats without needing a conversion software. A complete list of supported file types for ImageJ are provided online (http://rsbweb.nih.gov/ij/docs/guide/userguide-8.html). The fifth operation is performed using custom-made functions in MATLAB (2008a, The MathWorks, Natick, MA). This section provides a step-by-step guideline to implement BEAS method using these two softwares.

i. Despeckle Filter Operation

After opening the image to be processed, go to Noise>Despeckle from the Process menu as shown. Despeckle filtering does not require an input from the user, and it is performed automatically once selected.
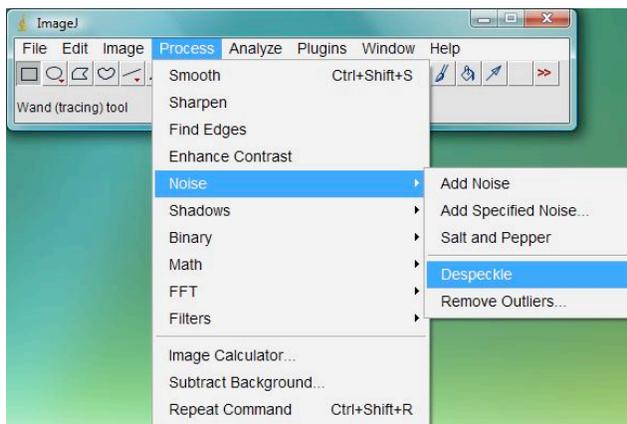
ii. Band-pass Filtering Operation

As the image is open, go to FFT>Bandpass Filter from the Process menu as shown. Bandpass

filtering requires input from the user. Please refer to ImageJ FFT Filter page (http://rsb.info.nih.gov/ij/plugins/fft-filter.html) for detailed explanation of input parameters. Band-pass filtering corrects for uneven illumination in the images by removing high frequency components from the image, and mitigates the effect of fibers, noise and/or other features (*e.g.*, those with size smaller than cell) by removing low frequency components. Input parameters can be changed to obtain best results in terms of achieving above goals. If the image to be processed does not suffer from such problems, this step can be skipped.
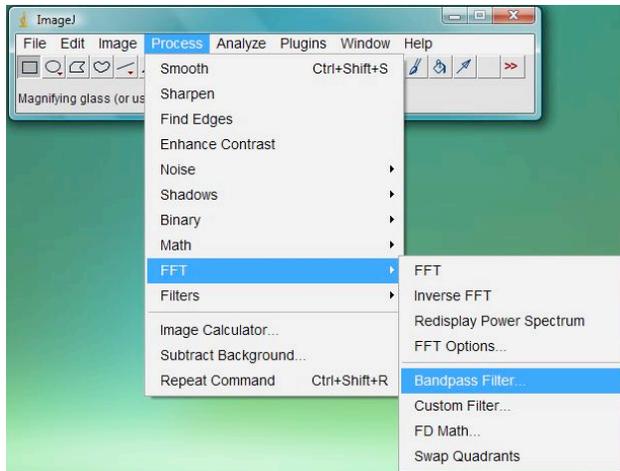
iii. Auto Local Thresholding

As the image is open, go to Adjust>Auto Local Threshold from the Image menu as shown.
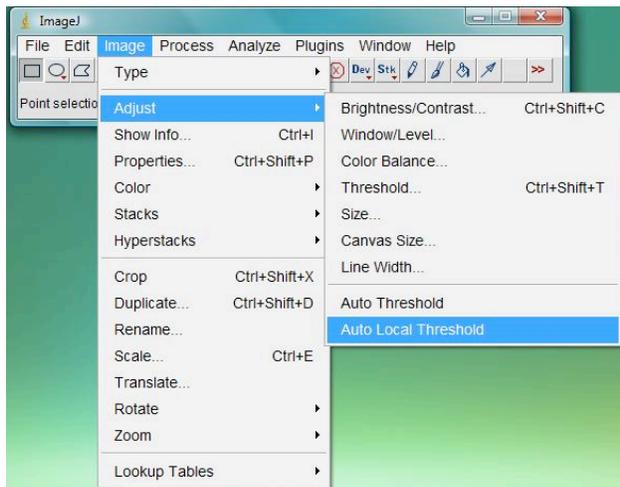
Select Sauvola as the method and change the Radius and special parameters in the menu to get desired results (selecting all the objects and rejecting all the background in the best case).
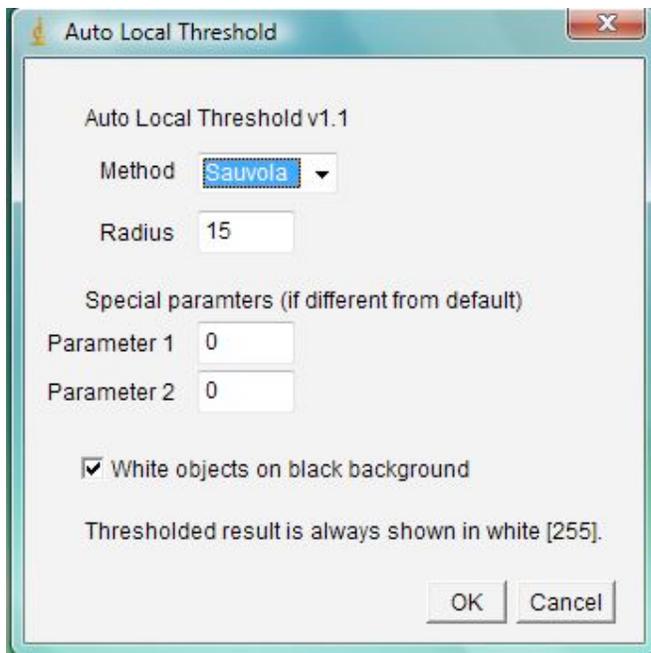
iv. Fill Holes and Open Operations
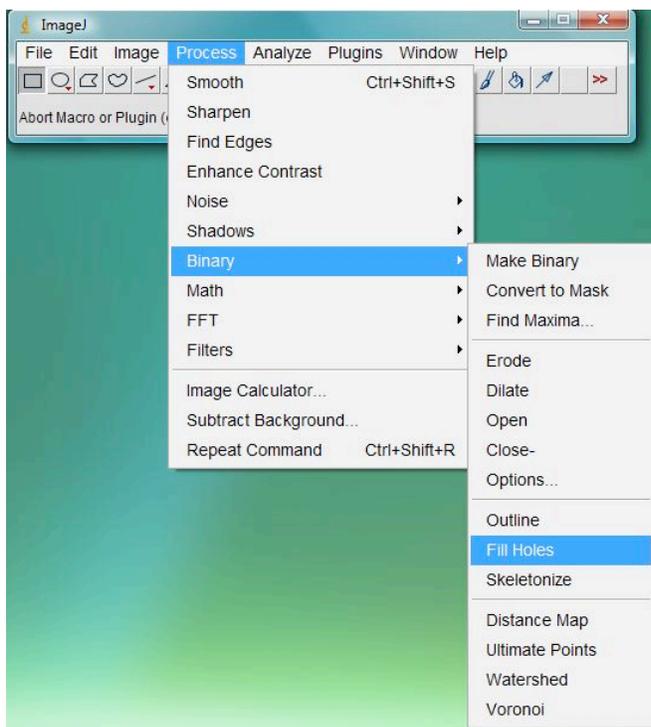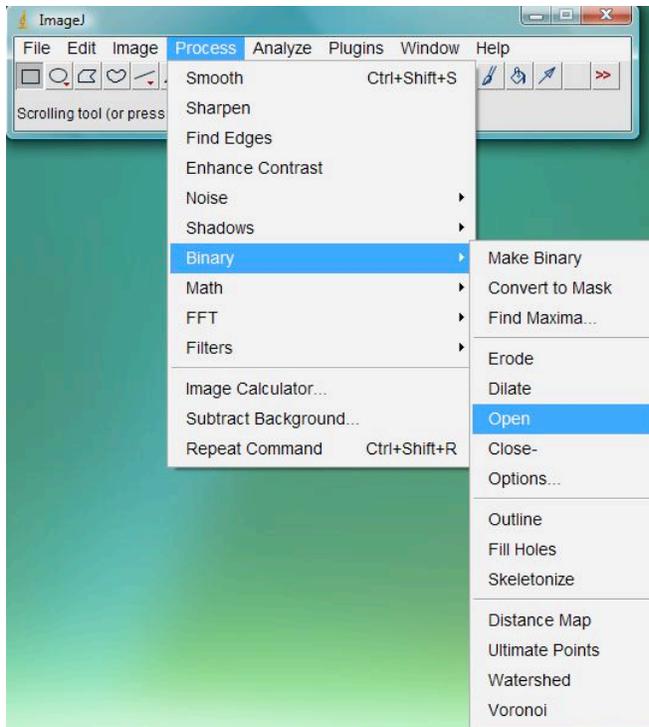
Perform fill holes and open operations from the Process bar as shown. If fill holes operation ends up in loosing objects in the image, first invert (Edit>Invert) then perform fill holes and invert back.

None of these two functions requires input from the user.

v. Extraction of orientation angle of the objects from the binary image

After saving the binary image using ImageJ, import it into MATLAB. Make sure your current directory has the files you need.

Type the following command to obtain the object orientation intensities in the binary image:

>> orientation_distribution("your_input_file")

without the quotes. Visual data showing the area weighted object orientation intensities will be generated like the following figure:
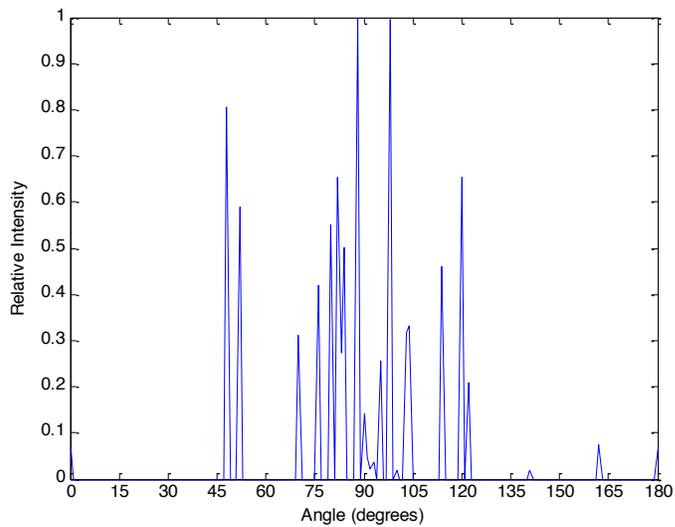
And finally, type the following command to obtain the alignment score:

>> calculate_alignment_score("your_input_file")

without the quotes. Output will look like:

alpha =

   1.5147

ans =

   0.7304

Here, alpha shows the degree of alignment in radians, and ans shows the calculated alignment score.

S.2. Results of the 15 images processed using our algorithm
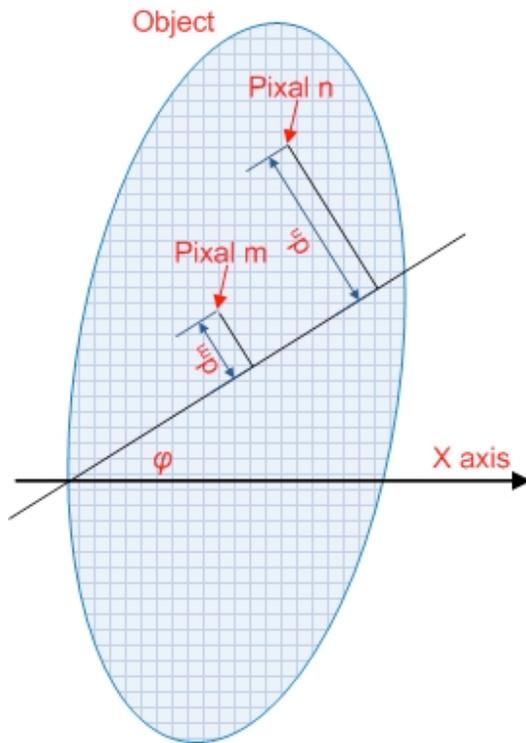
Figure S1. Schematic of the determination of object orientation.

(Image 1) Original   Pre-processed   Binarized
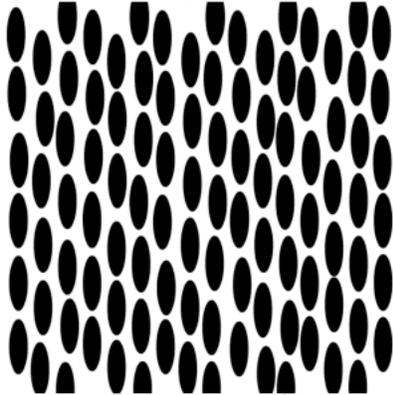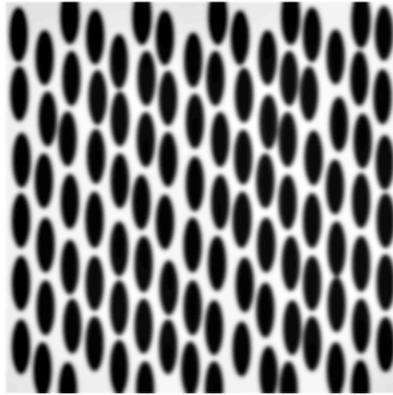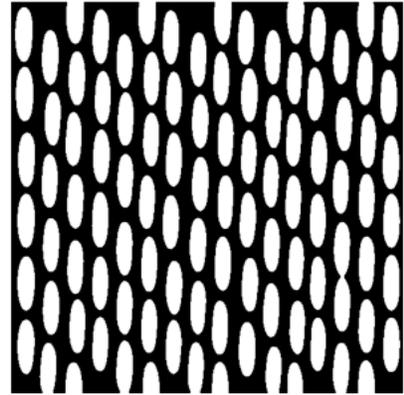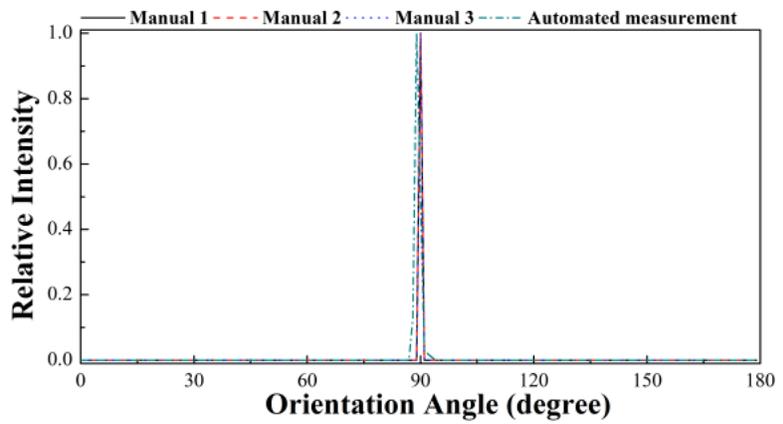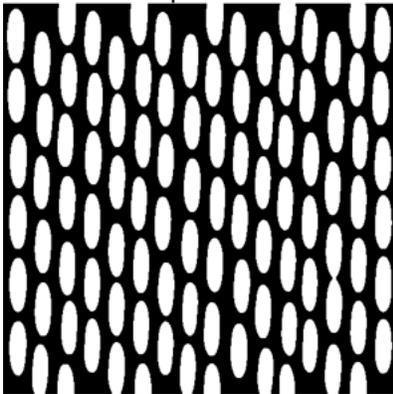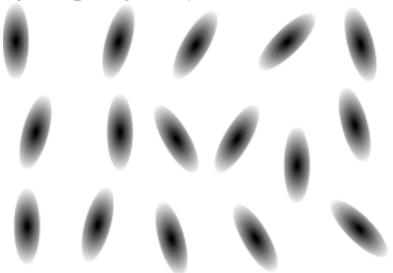
Post-processed

—— Manual 1   - - - Manual 2   ······ Manual 3   —·— Automated measurement

Relative Intensity

Orientation Angle (degree)

(Image 2) Original   Pre-processed   Binarized

Post-processed

—— Manual 1   - - - Manual 2   ······ Manual 3   —·— Automated measurement

Relative Intensity

Orientation Angle (degree)

(Image 3) Original   Pre-processed   Binarized

Post-processed

Manual 1   Manual 2   Manual 3   Automated measurement

(Image 4) Original   Pre-processed   Binarized

Post-processed

Manual 1   Manual 2   Manual 3   Automated measurement
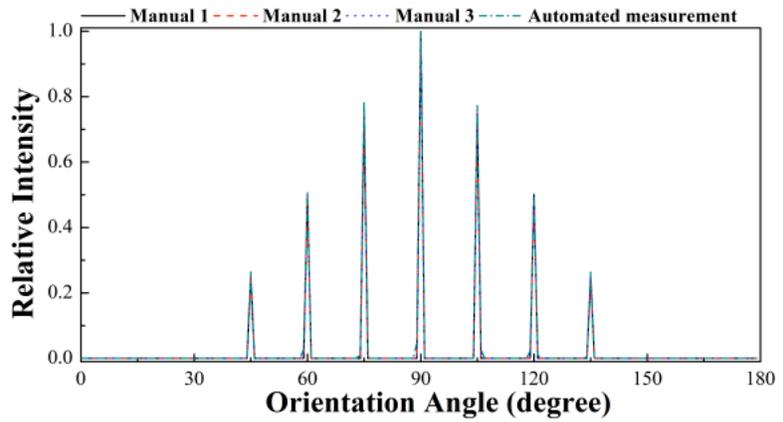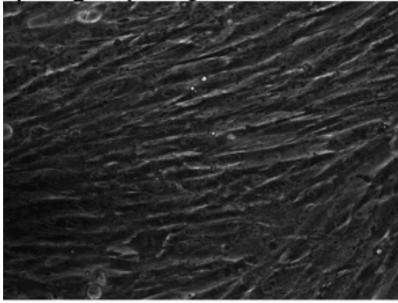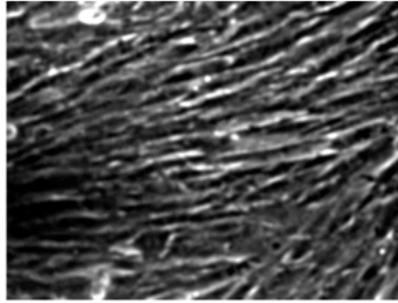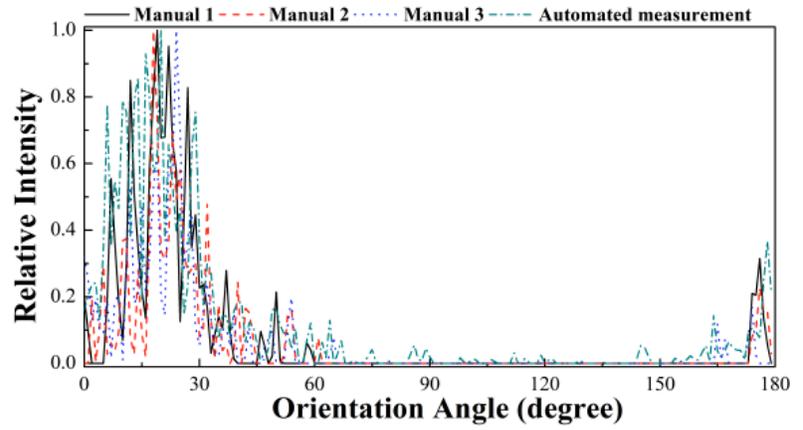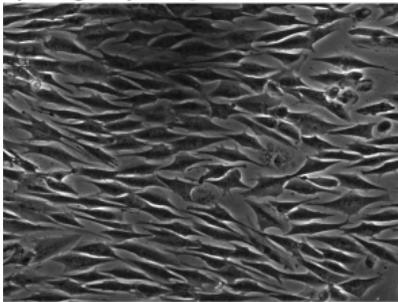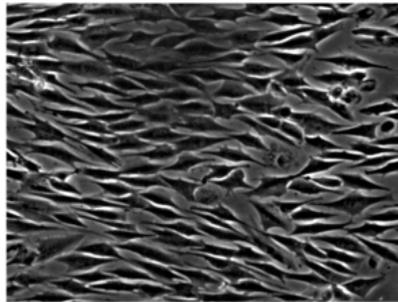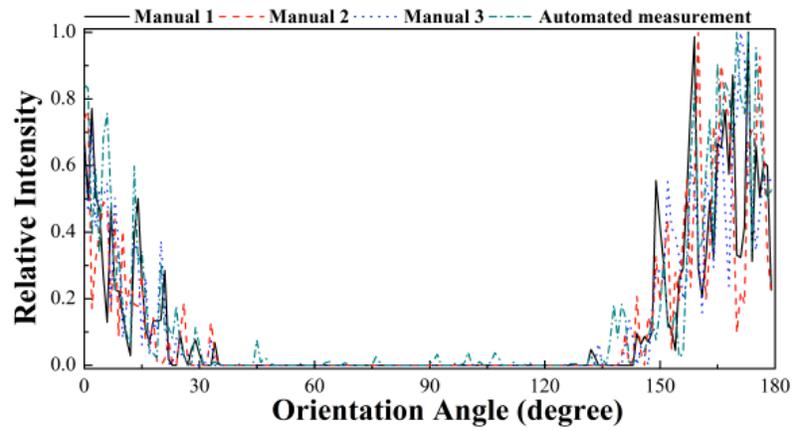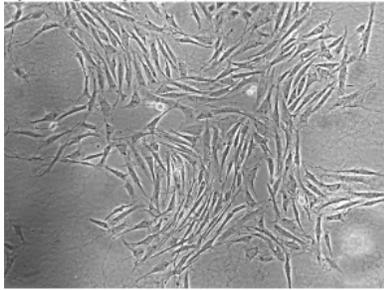
(Image 5) Original   Pre-processed   Binarized
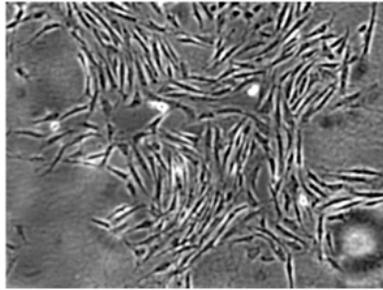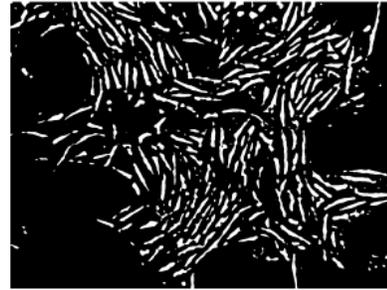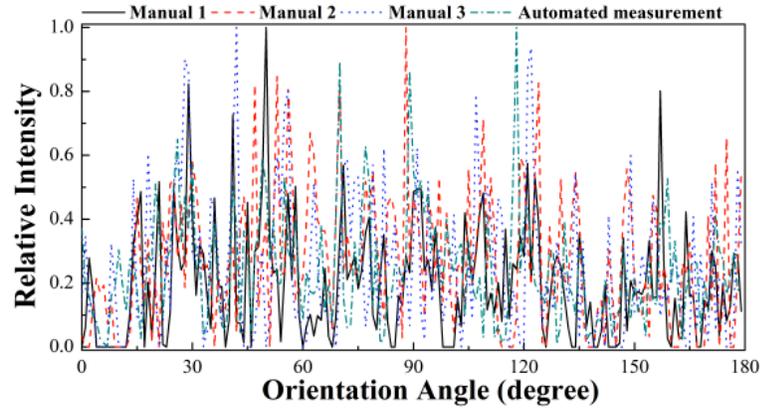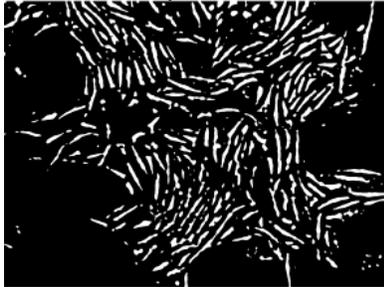
Post-processed

(Image 6) Original   Pre-processed   Binarized
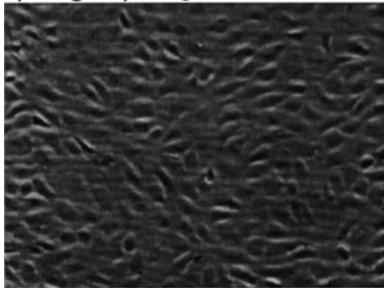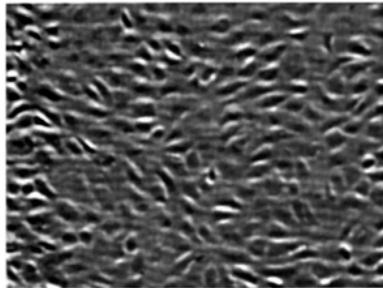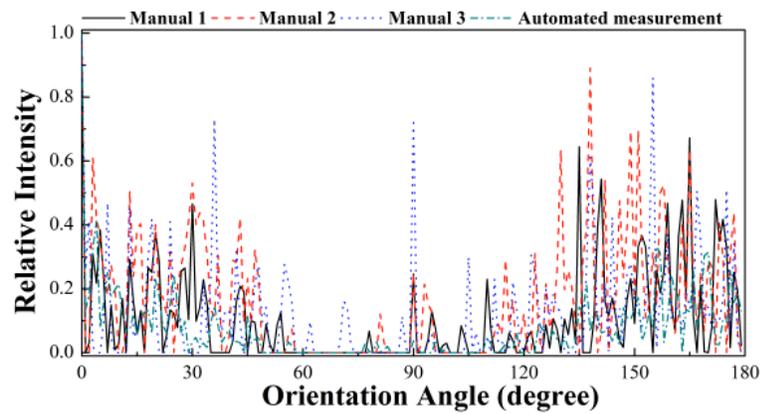
Post-processed
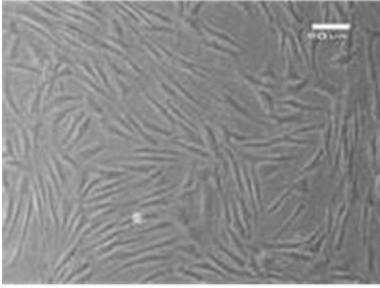
(Image 7) Original · Pre-processed · Binarized · Post-processed
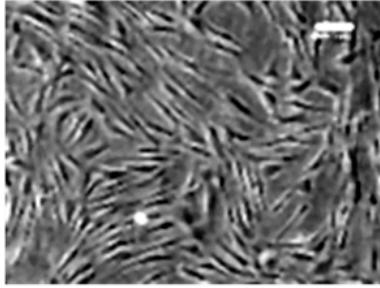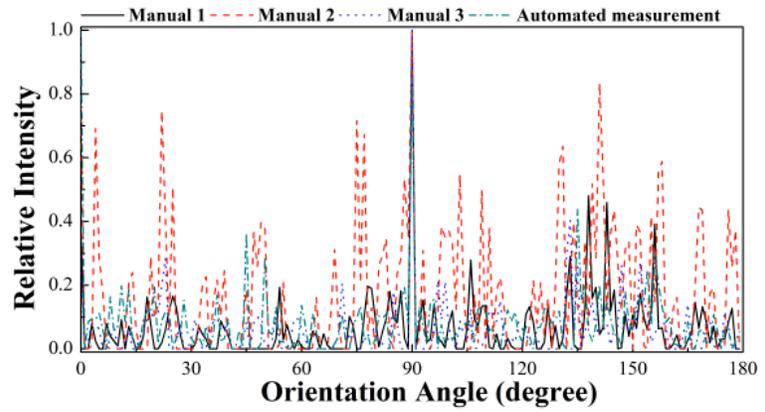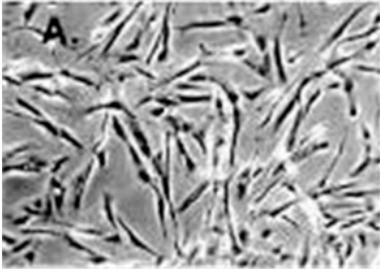
**(Image 8)** Original · Pre-processed · Binarized · Post-processed
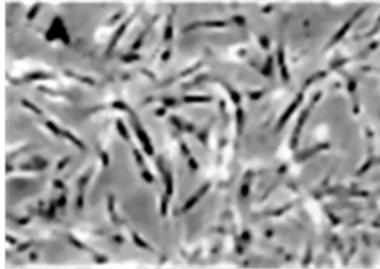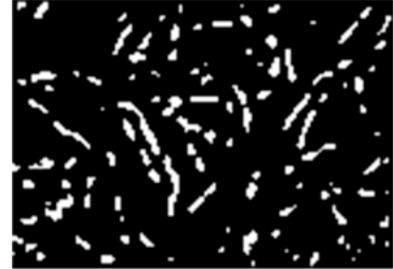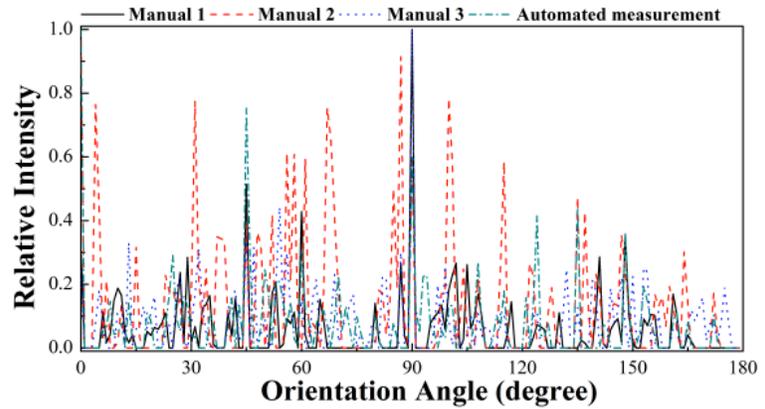
(Image 9) Original
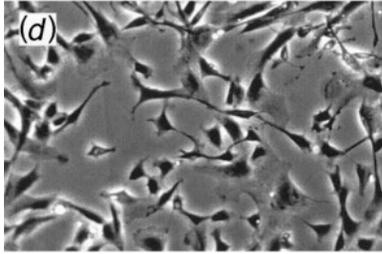
Pre-processed
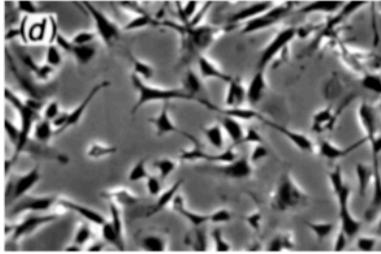
Binarized
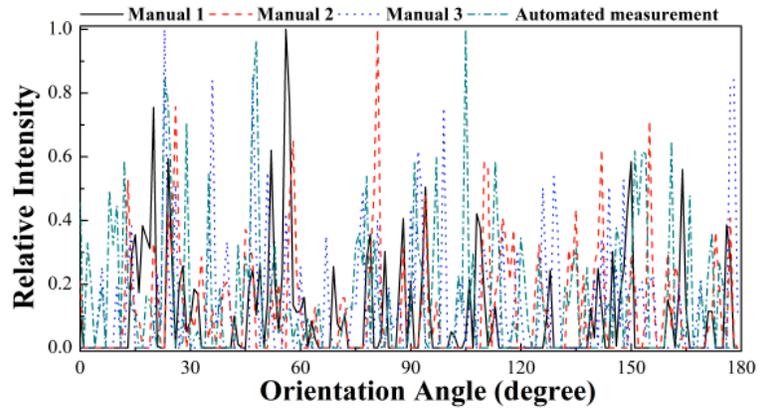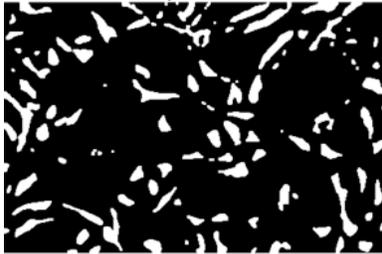
Post-processed

(Image 10) Original
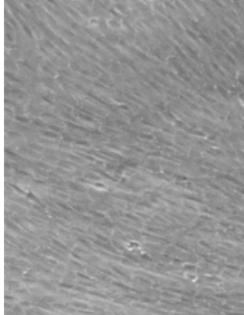
Pre-processed
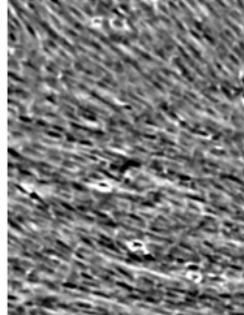
Binarized
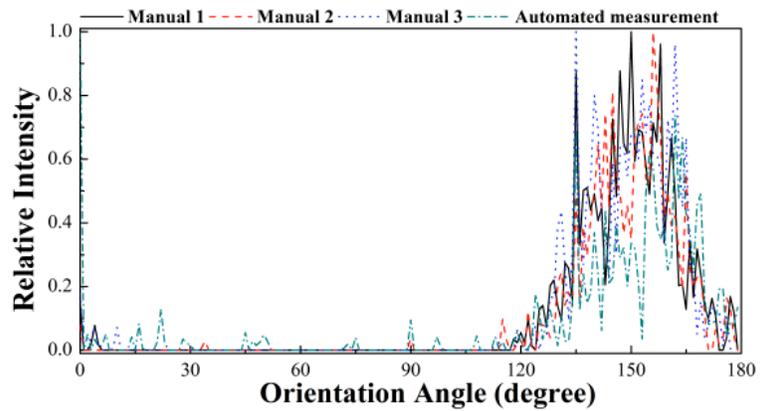
Post-processed
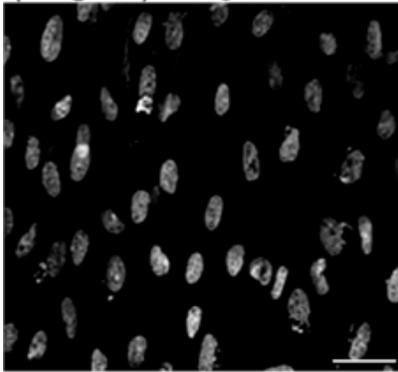
(Image 11) Original — Pre-processed — Binarized — Post-processed
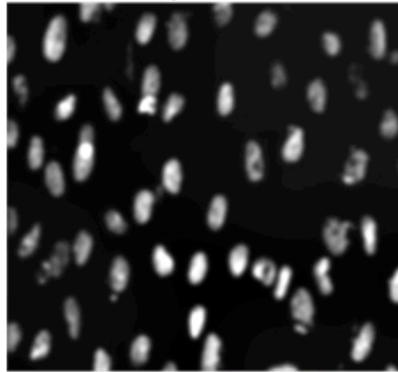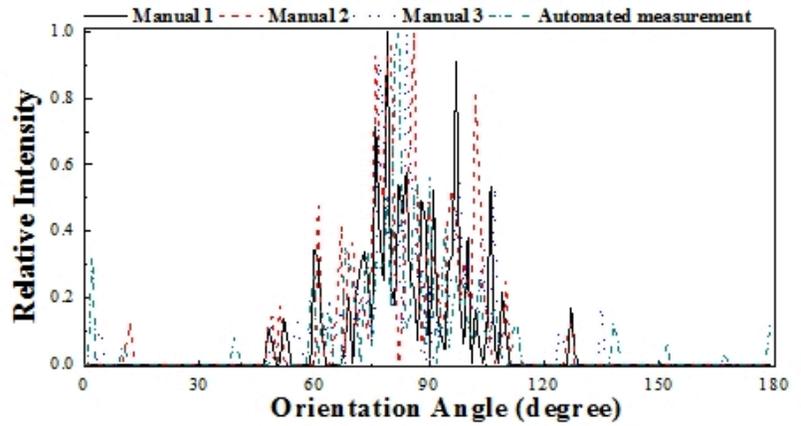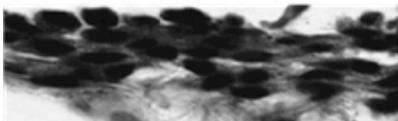
(Image 12) Original — Pre-processed — Binarized — Post-processed
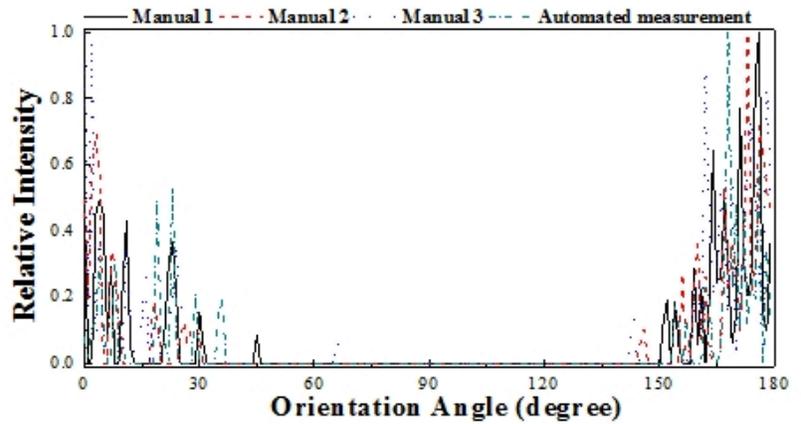
(Image 13) Original

Pre-processed

Binarized

Post-processed

Manual 1 — — Manual 2 ······ Manual 3 — · — Automated measurement

Relative Intensity

Orientation Angle (degree)
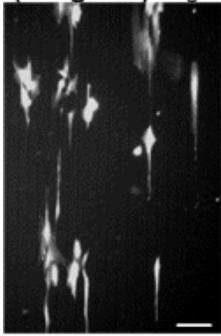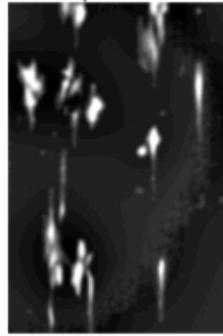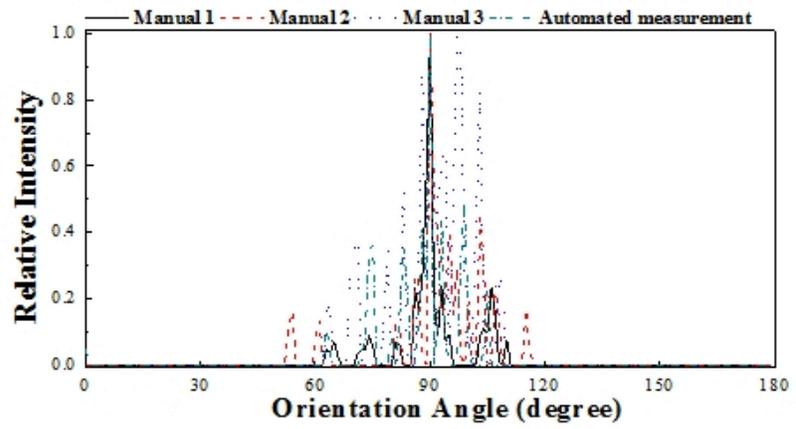
(Image 14) Original

Pre-processed

Binarized

Post-processed

Manual 1 — — Manual 2 ······ Manual 3 — · — Automated measurement

Relative Intensity

Orientation Angle (degree)
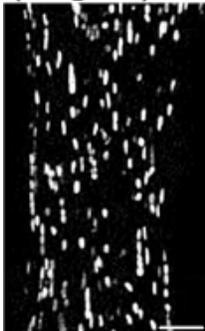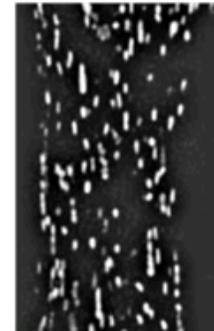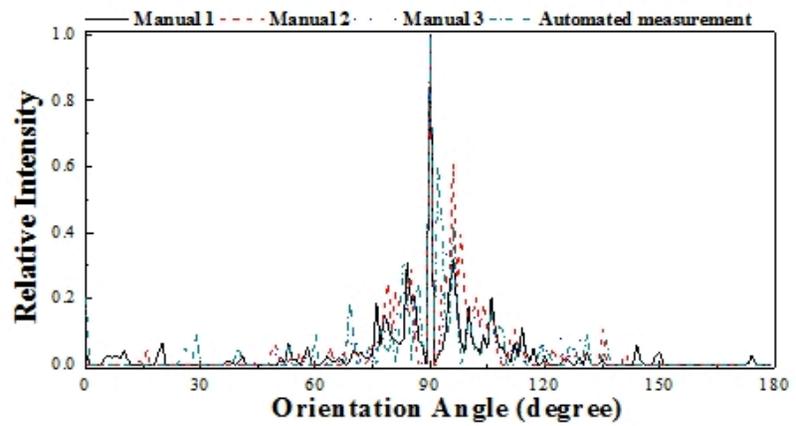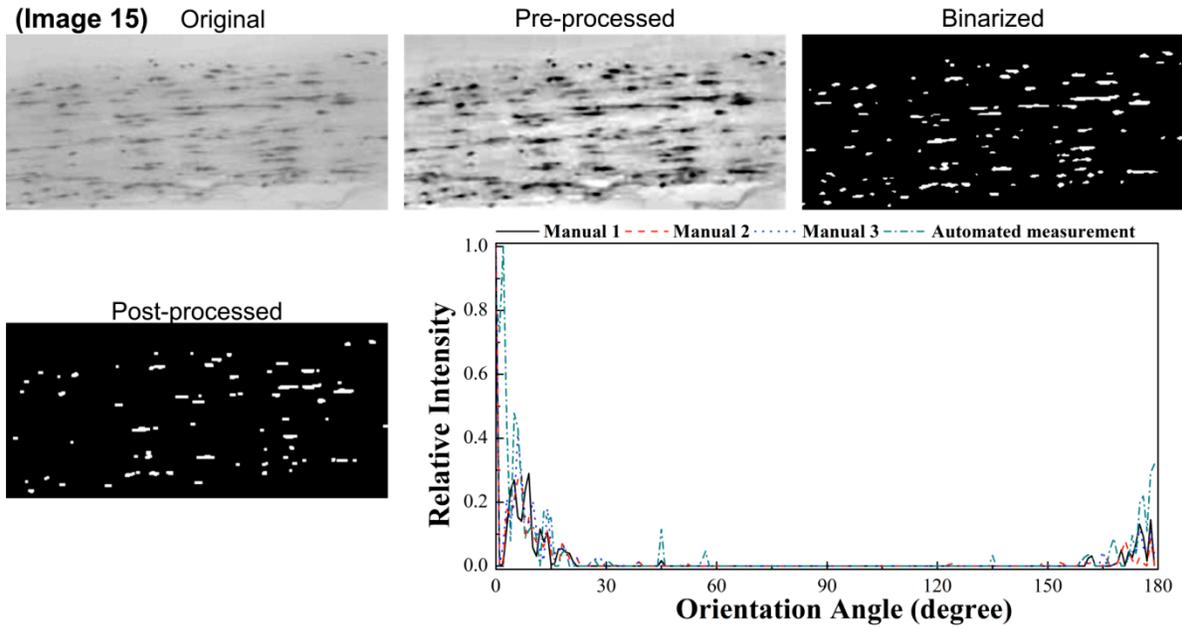
Figure S2. The steps of our image-processing method are demonstrated using the fifteen images referred to in Table S1. For each image, the original (upper left), pre-processed (upper middle), binarized (upper right) and post-processed (lower left) versions are shown, along with a graph of the image's orientation distribution. In binary images (the binarized and post-processed version of each image), objects are shown in white, and background in black. On each graph, the orientation distribution determined manually is shown in blue, the automated distribution weighted by object length in green, and the automated distribution weighted by object area in red. Relative intensity represents the total weight of all objects in each one-degree bin, divided by the weight in the highest-intensity bin for each method of measurement. Scale bar: 40 µm for image 11, 50 µm for image 13, 50 µm for image 14.
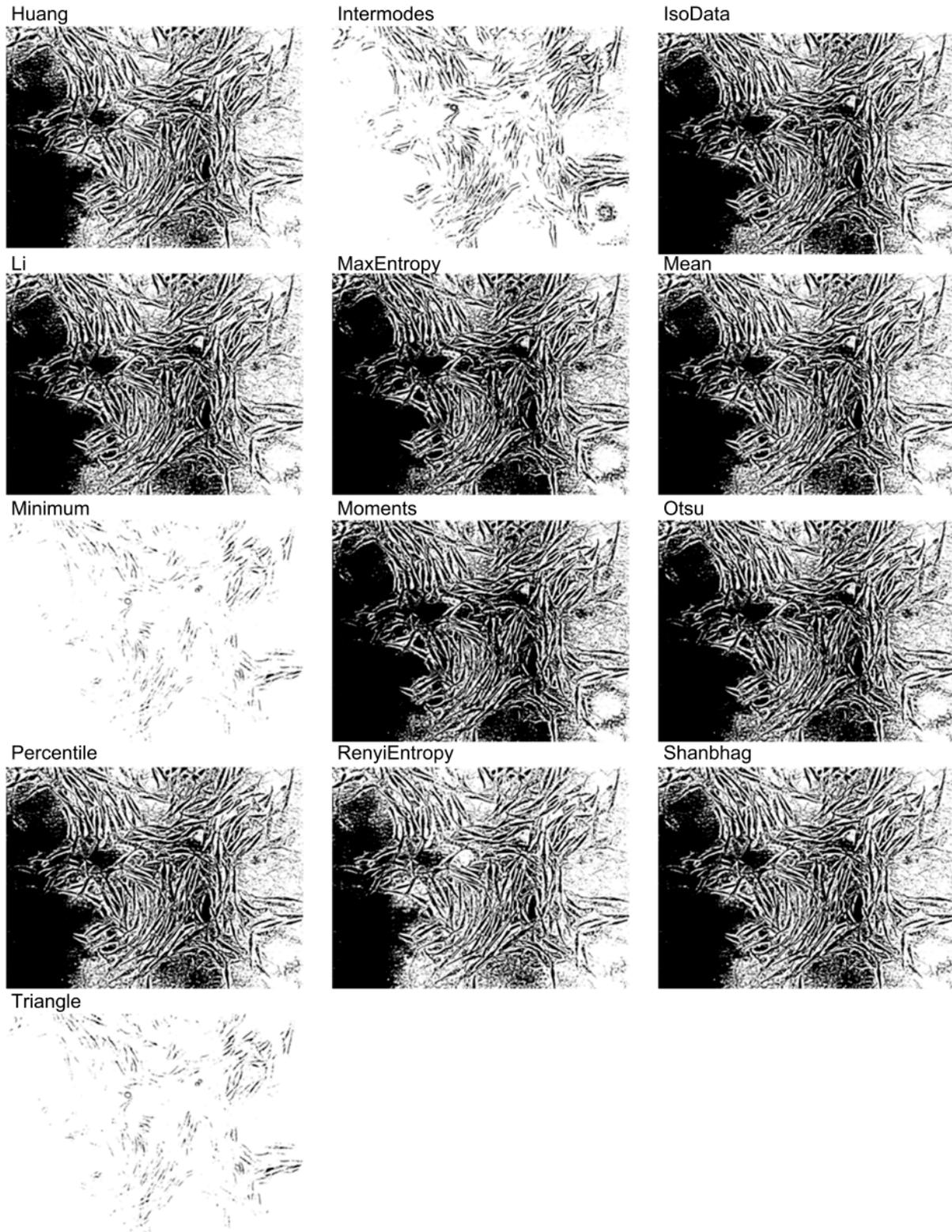
Figure S3. Results of various binarization methods. Using Landini's* software with ImageJ, several commonly used thresholding algorithms are utilized to obtain binary images from the original image in Figure 3a. The name of the algorithms are given as they appear in the

Landini's* software. Global threshold-based methods were found to be inadequate, as they either registered a large amount of background as cells, or missed large numbers of cells.

(a) Original Confocal Image

Green component

(b)

(c)

(d)

(e)

Blue component

(f)
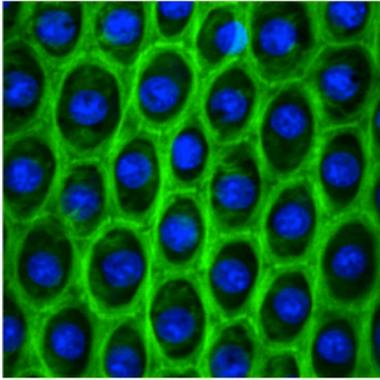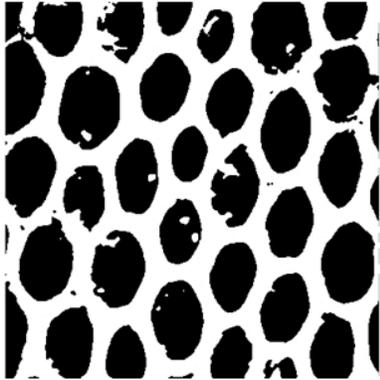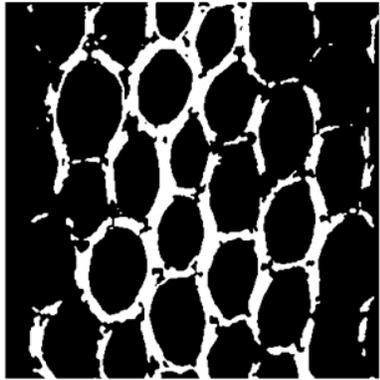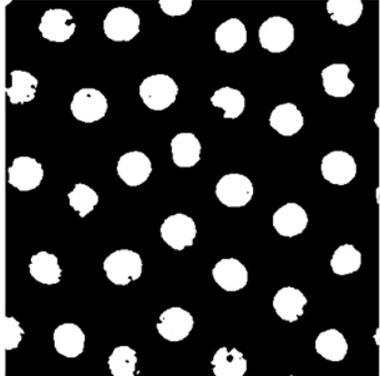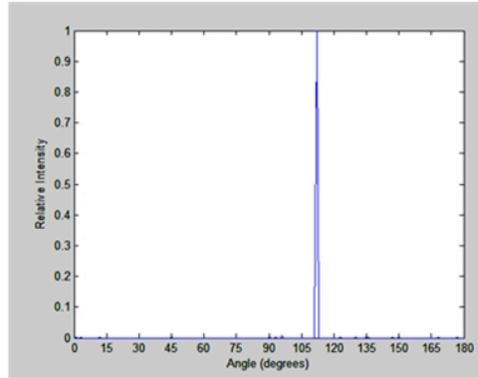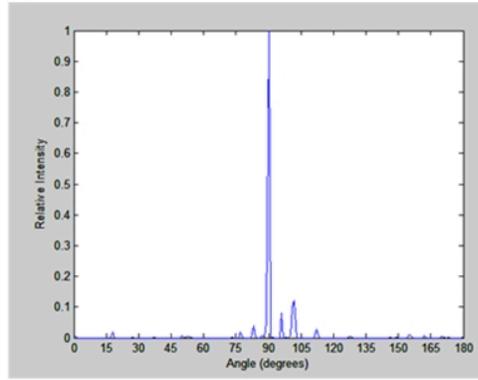
(g)
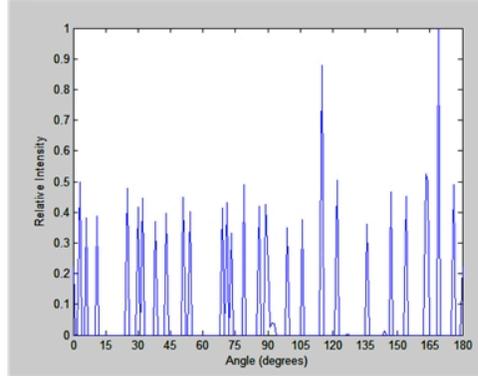
Figure S4. Quantification of alignment of retinal pigment epithelium (RPE) cells from a confocal image (a). Selecting the green objects, i.e. cytoskeleton, in the image yields the binary image **(b)**. However, note that it is continuous so program treats it as if it is a single object. The result of relative intensity shows a single peak at around 105 degrees **(c)**. Note that positive degree is defined as clockwise. By changing the threshold in the image yields the following binary image (**d**). Note that it is not continuous for this case, but some of the cells are lost. Result is multiple intensity components largest being around 90 degrees **(e)**. Selecting the blue objects, i.e. cell nuclei, in the image yields a binary image **(f)**. Since the objects appear circular in geometry, result gives multiple peaks **(g)**. The image was from NIH website:
http://www.nei.nih.gov/eyeonnei/snapshot/archive/051809.asp

Table S1. Description of images used in this study

Image #	Cell Type	Details about the image	Ref.
Image 1	Test image		
Image 2	Test image		
Image 3	Smooth muscle	Phase, 10x	
Image 4	Smooth muscle	Phase, 10x	
Image 5	Smooth muscle	Phase, 10x	
Image 6	Bovine aortic endothelial cells	Phase, 20x	(1)
Image 7	Rabbit esophagus SMC	light micrograph, 40x	(2)
Image 8	Canine vascular SMC	Phase	(3)
Image 9	Canine vascular SMC	Phase	(3)
Image 10	Smooth muscle	Phase, 10x	
Image 11	Rabbit corneal fibroblast nuclei	Green fluorescence	(4)
Image 12	SMC	H&E stain, RBG image, green channel, 100x	(5)
Image 13	Astrocyte	Green fluorescence	(6)
Image 14	Skeletal muscle	Green fluorescence (myogenin)	(7)
Image 15	Fibroblast	H&E stain, RGB image, photoshop greyscale, 20x	(8)

Table S2. Alignment Results of Images

Image #	Manual	BEAS	FFTRS	Gradient
1	1.000	1.000	0.038	0.680
2	0.700	0.696	0.215	0.369
3	0.911	0.847	0.012	0.335
4	0.887	0.876	0.019	0.530
5	0.413	0.135	0.003	0.042
6	0.455	0.639	0.017	0.391
7	0.186	0.113	0.003	0.064
8	0.142	0.177	0.005	0.054
9	0.079	0.035	0.003	0.013
10	0.914	0.793	0.026	0.432
11	0.868	0.838	0.005	0.242
12	0.906	0.863	0.016	0.478
13	0.929	0.947	0.035	0.447
14	0.830	0.757	0.027	0.471
15	0.958	0.936	0.039	0.644
μ	**0.679**	**0.643**	**0.346**	**0.031**
σ	0.329	0.344	0.218	0.053

Manual: Manual measurement
FTBE: Filtered Thresholding based Binarized Extraction
FFTRS: FFT radial sum method
Gradient: gradient method
μ: average
σ: standard deviation

Supplemental References

1. Karlon WJ, Hsu PP, Li S, Chien S, McCulloch AD, Omens JH. Measurement of orientation and distribution of cellular alignment and cytoskeletal organization. Ann Biomed Eng.27:712-20. 1999.
2. Cha JM, Park SN, Noh SH, Suh H. Time-dependent modulation of alignment and differentiation of smooth muscle cells seeded on a porous substrate undergoing cyclic mechanical strain. Artificial organs.30:250-8. 2006.
3. Lee AA, Graham DA, Dela Cruz S, Ratcliffe A, Karlon WJ. Fluid shear stress-induced alignment of cultured vascular smooth muscle cells. J Biomech Eng.124:37-43. 2002.
4. Wray LS, Orwin EJ. Recreating the microenvironment of the native cornea for tissue engineering applications. Tissue engineering.15:1463-72. 2009.
5. Kim BS, Nikolovski J, Bonadio J, Mooney DJ. Cyclic mechanical strain regulates the development of engineered smooth muscle tissue. Nat Biotechnol.17:979-83. 1999.
6. Recknor JB, Recknor JC, Sakaguchi DS, Mallapragada SK. Oriented astroglial cell growth on micropatterned polystyrene substrates. Biomaterials.25:2753-67. 2004.
7. Bian W, Bursac N. Engineered skeletal muscle tissue networks with controllable architecture. Biomaterials.30:1401-12. 2009.
8. Henshaw DR, Attia E, Bhargava M, Hannafin JA. Canine ACL fibroblast integrin expression and cell alignment in response to cyclic tensile strain in three-dimensional collagen gels. J Orthop Res.24:481-90. 2006.